crystals

MDPI

Article

Space Group Choice for an Octahedral Zn Complex with Nalidixic Acid and (*R*, *R*)-Diaminocyclohexane as Ligands: Get the Stereochemistry Right

Martin Lutz * and Tom W. Müller

Structural Biochemistry, Faculty of Science, Utrecht University, Universiteitsweg 99, 3584 CG Utrecht, The Netherlands
* Correspondence: m.lutz@uu.nl; Tel.: +31-06-22735980

Abstract: With this report, the space group of $[Zn(Nal)(DACH)_2]Cl$ is corrected (*Nal*: nalidixic acid mono-anion; *DACH*: diaminocyclohexane) from its wrong description in the literature. In the correct, non-centrosymmetric space group $P1$, the crystal structure is well ordered and the stereochemistry is correct. Crystallographic tools to recognize the correct symmetry are described. This work encourages experienced and inexperienced scientists to remain critical about the output of automatic, black-box crystallographic software.

Keywords: chelate complex; chirality; enantiopurity; space group; absolute structure

Citation: Lutz, M.; Müller, T.W. Space Group Choice for an Octahedral Zn Complex with Nalidixic Acid and (*R*, *R*)-Diaminocyclohexane as Ligands: Get the Stereochemistry Right. *Crystals* **2024**, *14*, 498. https://doi.org/10.3390/cryst14060498

Academic Editor: Alexander Y. Nazarenko

Received: 5 May 2024
Revised: 19 May 2024
Accepted: 22 May 2024
Published: 24 May 2024

1. Introduction

Enantiopure *trans*-1,2-diaminocyclohexane (DACH) and its derivatives are inexpensive and common reagents in asymmetric synthesis [1] and chiral resolution, for example, in chromatography [2] or through the formation of diastereomeric co-crystals [3]. In the context of research on therapeutical applications of the antibiotic molecule nalidixic acid (NalH, 1-ethyl-7-methyl-4-oxo-1,4-dihydro-1,8-naphthyridin-3-carboxylic acid), Arjmand et al. published in 2014 the X-ray crystal structure of the octahedral complex $[Zn(Nal)(DACH)_2]Cl$ [4]; see Scheme 1. They reported two independent metal complex molecules in the asymmetric unit which are both in Λ configuration at the chelated Zn atoms. Because the structure is described in the centrosymmetric space group $P\bar{1}$ (no. 2), the inverted configurations are equally present in the unit cell.

According to Neumann's principle, which is a fundamental postulate in crystallography, all physical properties of a crystal are related to the symmetry of the crystal [5]; for physical applications of organic crystals, symmetry research on the polar axis is an active field, cf. [6]. Crystallographers therefore do their utmost effort to establish the correct space group symmetry. In addition to the physical properties, the selection of the wrong space group can have severe chemical effects. Examples for chemical consequences are given in [7]. The most common space group errors are missed symmetry, i.e., the symmetry is too low. Modern software tools should help to avoid these errors [8]. Cases with too high symmetry are rare [9]. Often, they can be detected by the presence of disorder and by high R values. To the best of our knowledge, automatic software tools for the detection of too high symmetry are not available.

For the synthesis of $[Zn(Nal)(DACH)_2]Cl$ in [4], the authors used 1*R*,2*R*-diaminocyclohexane. It is well known that enantiopure (enantiomerically pure) molecules can only crystallize in a space group belonging to one of the 65 Sohncke types [10]. A Sohncke-type space group contains no operations of the second kind, i.e., no handedness-reversing operations. We have recently documented in a similar case that when a centrosymmetric space group is erroneously chosen for an enantiopure material, the description and refinement of

the crystal structure will have severe disorder and physically unreasonable atomic displacement parameters [11]. In the case of $[Zn(Nal)(DACH)_2]Cl$, the erroneous introduction of an inversion center in [4] is only possible when equal amounts of the Λ- and Δ configuration of the octahedral chelate complex are present in the crystal structure. The synthetic procedure does not exclude this. But the inversion center will also lead to the presence of equal amounts of the 1*R*,2*R*- and the 1*S*,2*S*-form of the diaminocyclohexane ligand. This is not possible if an enantiopure starting material has been used and no racemization has taken place. Consequently, the metal complex molecules in the crystal structure in [4] show severe disorder and very large anisotropicity of the atomic displacement parameters. Additionally, there are non-coordinated fragments described in [4] which are chemically not identifiable. The reflection data in [4] are rather weak with a percentage of observed reflections with $I > 2\sigma(I)$ of only 28%.

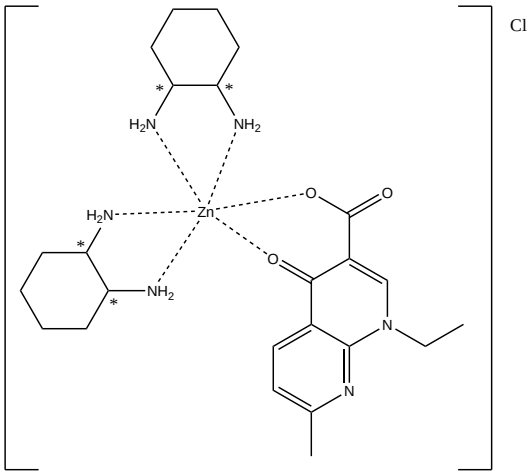

Scheme 1. Molecular structure in **1a** and **1b**.

The publication of [4] does not contain X-ray reflection data in the Supplementary Materials or the data deposition. It was therefore not possible to redetermine the structure on the original data. For a correct space group determination and proper crystal structure description, we consequently had to re-synthesize the crystals and perform a new single-crystal X-ray diffraction experiment. The description in the correct, non-centrosymmetric space group *P*1 (no. 1) will be reported in the current article.

2. Materials and Methods

2.1. Synthesis and Crystallization

First, 0.463 g (1.99 mmol) nalidixic acid (NalH) was suspended in 10 mL ethanol and 2 mL water. Then, 0.149 g (2.66 mmol) of potassium hydroxide (KOH) in 3 mL of water was slowly added under stirring. Following this, 20 mL ethanol was added to improve the dissolution. Then, 0.456 g (3.99 mmol) 1*R*,2*R*-diaminocyclohexane in 10 mL ethanol was added. Finally, 0.276 g (2.02 mmol) zinc(II)chloride in 10 mL water was added. A clear solution was obtained. Within three days, crystals of **1a** had formed by slow evaporation at room temperature.

Before recrystallization, crystals of **1a** were dried on filter paper by standing in open air for three days. Then, they were dissolved in 5 mL of a mixture of methanol–chloroform (8:2) by heating to 60 °C. Crystals of **1b** formed after two hours of standing at room temperature.

2.2. X-ray Data Collection

Photographs of the crystals **1a** and **1b** and approximate descriptions of their shape are given in Figures S1–S3 in the Supplementary Materials. X-ray reflection data were measured on a Bruker ApexII diffractometer with sealed tube and Triumph monochromator. For **1a** and **1b**, 4105 frames were measured, respectively, in 11 ω scans with a detector distance of

45 mm and a rotation increment of 0.3°. The intensity integration was performed with the Eval15 software [12]. The profile prediction in Eval15 involved an isotropic mosaicity of 0.25° for both crystals **1a** and **1b**. Small interfering contributions from additional crystallites were ignored in the case of **1b**.

The SADABS program [13] was used for multiscan absorption correction and scaling. The Laue symmetry $\overline{1}$ was input for the parameter refinement and scaling, and the point group symmetry 1 for the error model and statistics.

2.3. Structure Solution and Refinement

Structure refinement was performed with the SHELXL-2019/3 software [14]. The atomic coordinates of [4] were expanded to space group $P1$ and were taken as starting model for **1a** and **1b**. The coordinates of the minor disorder components of the $DACH$ ligands, the chlorine atoms, and the solvent molecules were deleted. The chlorine atoms and the solvent molecules were re-determined later from difference Fourier maps. In the initial refinement cycles, distances and angles in the metal complex molecules were restrained with the SHELXL instruction SAME. These restraints were released in later stages of the refinement. For the convergence of the refinement, some atoms in the $DACH$ ligands needed to be shifted manually from the starting model to the correct positions.

Hydrogen atoms were introduced in calculated positions. For the metal complex molecules, they were refined with a riding model. For the solvent molecules, the hydrogen positions were calculated based on potential hydrogen bond acceptors. These hydrogen atoms were kept fixed during the refinement. Overall, the model of the disordered solvent remained deficient. Also, the possible minor disorder of the chlorine atoms was ignored.

Geometrical calculations and checking for higher symmetry was performed with the PLATON software [8]. Further experimental details about the crystal structure determinations are given in Table 1.

Table 1. Experimental details of the crystal structures. An atomic model for the disordered solvent in **1a** and **1b** was used.

	AYAT [4]	**1a** [1]	**1b**
sum formula	$C_{48}H_{74}Cl_2N_{12}O_{12}Zn_2$	$[C_{24}H_{39}N_6O_3Zn]Cl \cdot 2.75(H_2O)$	$[C_{24}H_{39}N_6O_3Zn]Cl \cdot 1.75(CH_3OH) \cdot 0.375(H_2O)$
formula weight	1212.83	609.97	623.26
crystal system	triclinic	triclinic	triclinic
space group	$P\overline{1}$ (no. 2)	$P1$ (no. 1)	$P1$ (no. 1)
a [Å]	12.0599(7)	12.11092(18)	12.2267(2)
b [Å]	12.4700(5)	12.03184(18)	12.29289(18)
c [Å]	21.0570(10)	21.5533(3)	21.5785(4)
α [°]	80.753(4)	80.549(1)	79.909(1)
β [°]	85.925(4)	84.981(1)	83.792(1)
γ [°]	73.453(4)	73.182(1)	72.942(1)
V [Å^3]	2995.0(3)	2962.88(8)	3047.08(9)
Z	2	4	4
D_x [g/cm^3]	1.345	1.367	1.359
μ [mm^{-1}]	0.96	0.97	0.94
T [K]	100(2)	150(2)	150(2)
crystal size [mm]	0.36 × 0.29 × 0.14	0.41 × 0.27 × 0.06	0.29 × 0.15 × 0.09
λ [Å]	0.71073	0.71073	0.71073
$(\sin\theta/\lambda)_{max}$ [Å^{-1}]	0.64	0.65	0.65
meas. refl.	23,434	74,146	76,172
unique refl.	12,452	27,263	27,951
obs. refl. [$I > 2\sigma(I)$]	3526	23,576	22,793
R_{int}	0.088	0.026	0.030
no. parameters	650	1378	1441
no. restraints	4	75	127

Table 1. *Cont.*

	AYAT [4]	**1a** [1]	**1b**
a, b [†]	0.1444, 0.0000	0.0676, 1.1135	0.0596, 0.3522
R1/wR2 (obs. refl.)	0.0941/0.2340	0.0400/0.1139	0.0380/0.1021
R1/wR2 (all refl.)	0.2794/0.2881	0.0468/0.1175	0.0501/0.1079
S	0.803	1.079	1.080
Flack x [15]	–	0.000(9)	−0.015(9)
Parsons z [16] (SHELXL)	–	0.003(4) [10,455 pairs]	0.014(4) [9808 pairs]
Parsons z [16] (PLATON)	–	0.014(3) [10,634 pairs]	0.011(3) [9995 pairs]
Hooft y [17] (PLATON)	–	0.000(1) [13,631 pairs]	0.025(1) [13,974 pairs]
$\Delta\rho_{min/max}$ [e/Å^3]	−0.61/1.13	−0.90/1.88	−0.49/0.96

[1] For a better comparison, the triclinic unit cell of **1a** is in a non-reduced setting. [†] a and b are parameters of the SHELXL weighting scheme $w = 1/[\sigma^2(F_o^2) + (a \times P)^2 + b \times P]$ with $P = (F_o^2 + 2F_c^2)/3$.

2.4. Application of Squeeze

For a better treatment of the diffuse solvent regions, the Squeeze algorithm [18] was used. The metal complex molecules and the chloride anions were considered to be the ordered part of the structure. The water and methanol molecules were considered disordered and were removed from the atomic model. The solvent accessible region was then determined with a default probe radius of 1.20 Å. Prior to the calculation of the diffuse electron density, the reflection data were merged according to the point group symmetry 1. For every reflection, the A- and B-terms of the diffuse solvent contribution were calculated by PLATON and read by SHELXL (with the instruction ABIN). With this procedure, the observed structure factors F_{obs}^2 are left unchanged, and the solvent contribution only affects the calculated structure factors F_{calc}^2.

The Squeeze calculation showed significant residual density excursions in the ordered part of the structure between −0.9 and 1.2 e/Å^3 in **1a**. Further details about the Squeeze results are given in Table 2.

Table 2. Refinement results after the application of Squeeze [18].

	1a-Squeeze	**1b-Squeeze**
solvent accessible voids [Å^3]	174 + 148	261 + 181
electron count in voids	57 + 59	75 + 61
no. parameters	1270	1270
no. restraints [1]	3	3
a, b [†]	0.0528, 0.4115	0.0393, 0.0000
R1/wR2 (obs. refl.)	0.0353/0.0947	0.0313/0.0754
R1/wR2 (all refl.)	0.0420/0.0975	0.0423/0.0791
S	1.119	1.067
Flack x [15]	0.000(8)	0.005(6)
Parsons z [16] (SHELXL)	0.003(3) [10,468 pairs]	0.010(4) [9840 pairs]
Parsons z [16] (PLATON)	0.245(2) [10,634 pairs]	0.148(3) [9996 pairs]
Hooft y [17] (PLATON)	−0.001(4) [13,631 pairs]	0.013(1) [13,974 pairs]
$\Delta\rho_{min/max}$ [e/Å^3]	−0.83/1.39	−0.31/0.29

[1] Floating origin restraints. [†] a and b are parameters of the SHELXL weighting scheme $w = 1/[\sigma^2(F_o^2) + (a \times P)^2 + b \times P]$ with $P = (F_o^2 + 2F_c^2)/3$.

2.5. Absolute Structure Determination

In all four cases **1a**, **1a-squeeze** , **1b** and **1b-squeeze**, the Flack x-parameter [15] was obtained by refinements as the inversion twin (i.e., with the SHELXL instructions TWIN and BASF). The Parsons z-parameter [16] and the Hooft y-parameter [17] were obtained by post-refinement determinations using SHELXL [14] and PLATON [8], respectively, after single-crystal refinements (i.e., without the instructions TWIN and BASF).

3. Results and Discussion

The aim of the current study was to re-synthesize $[Zn(Nal)(DACH)_2]Cl$ and to determine the correct space group in the crystal structure of this enantiopure complex. From the unit cell parameters in Table 1, we see a high similarity between **1a** and **1b** and the literature structure of [4], from now on called **AYAT** . For a quantitative comparison, spontaneous strain values S [19] were calculated, resulting in low values of 0.01329 for **1a** with **AYAT** and 0.01516 for **1b** with **AYAT**. The structural identity was further supported by the fact that the atomic coordinates of **AYAT** (expanded to space group $P1$) can be used as starting values for the structure determinations of **1a** and **1b**.

A detailed comparison of **1a** and **1b** with **AYAT** is not possible because the metal complex molecules in **AYAT** are severely disordered, and additional fragments in **AYAT** are chemically not identifiable. A calculation of the shortest non-bonding $Zn\cdots Cl$ distances in Table 3 reveals that there are significant differences in the packing despite the overall structural similarity. A graphical representation of the Zn and Cl atoms is given in Figure S4 in the Supplementary Materials. This can be explained by the fact that the chloride anions are part of the solvent region (vide infra), which appears to be rather variable between the different structures.

Table 3. Shortest $Zn\cdots Cl$ distances [Å].

AYAT [4]	**1a**	**1b**
4.345(3)	4.823(2)	4.2841(15)
4.348(4)	4.861(2)	4.2843(18)
4.377(3)	4.892(2)	4.3005(18)
4.415(4)	4.909(2)	4.3199(14)
	5.201(3)	4.3563(18)
	5.224(2)	4.3863(19)
	5.2680(19)	4.4695(18)
	5.3688(19)	4.5228(17)

3.1. Stereochemistry

In space group $P1$ of **1a** and **1b**, there are four independent Zn-complex molecules in the unit cell. None of the Zn-complex molecules show disorder. Consistent with **AYAT**, two molecules have a Λ configuration at the metal (Figure 1), and two have a Δ configuration (Figure 2). The archetypical octahedral $M(en)_3$ Werner complexes (en = ethylenediamine) have ideally a D_3 symmetry. The same D_3 symmetry holds for the corresponding $M(DACH)_3$ complexes [20]. In $[Zn(Nal)(DACH)_2]Cl$, one $DACH$ ligand is replaced by the achiral Nal ligand. A threefold symmetry is consequently not possible. If we ignore the details of the Nal ligand, we find an approximate C_2 symmetry for the octahedra at the Zn atoms (Figure 3).

Four independent Zn-complex molecules consequently have eight independent $DACH$ ligands. The cyclohexane rings are all in chair conformation and are very similar. The five-membered chelate rings at the Zn-center show significant conformational flexibility (Figure 4). The numerical values of the ring puckering analysis are provided in Tables S1 and S2 in the Supplementary Materials. The N–C–C–N torsion angles are in a *gauche* conformation and are rather constant with values between $-50.5(5)$ and $-56.8(5)^\circ$ for **1a** (Table 4) and between $-52.7(5)$ and $-56.6(5)^\circ$ for **1b** (Table 5). Importantly, all N–C–C–N torsion angles have a negative sign, and a λ conformation can be assigned to all eight chelate rings. We conclude that the enantiopurity of the $DACH$ ligands does not predetermine the configuration of the metal in **1a** and **1b**: both the Λ- and the Δ configurations are present in the two crystal structures. The enantiopure quality does predetermine the conformation of the five-membered chelate rings: they are all in λ conformation. The Λ and Δ complexes are thus not enantiomers and cannot be related by second-kind symmetry operations. Instead, they are $\Lambda-\lambda\lambda$ and $\Delta-\lambda\lambda$ diastereomers.

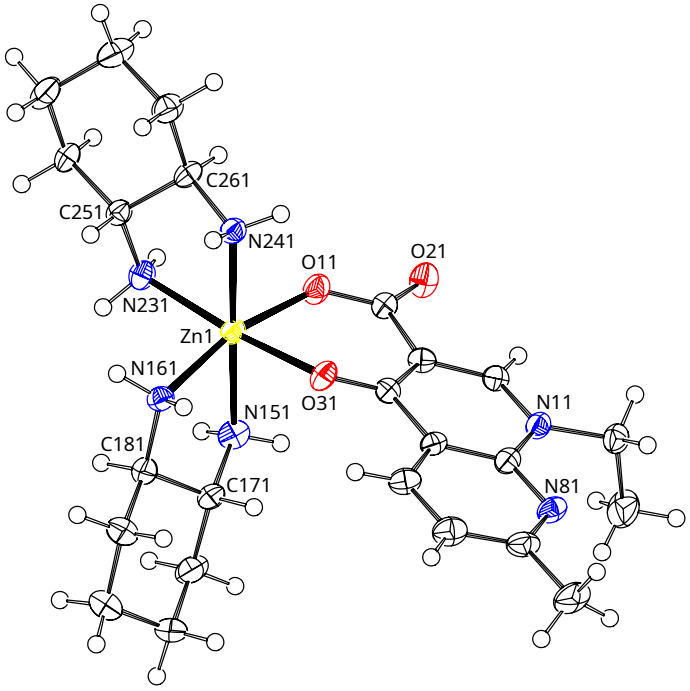

Figure 1. Displacement ellipsoid plot of the monocationic complex molecule at *Zn*1 in **1a** (ellipsoids at the 50% probability level). Atoms C171, C181, C251 and C261 are in *R* configuration. The metal environment has a Λ configuration. The complex at Zn3 is not shown but has the same configuration at the metal and the *DACH* ligands as at Zn1.

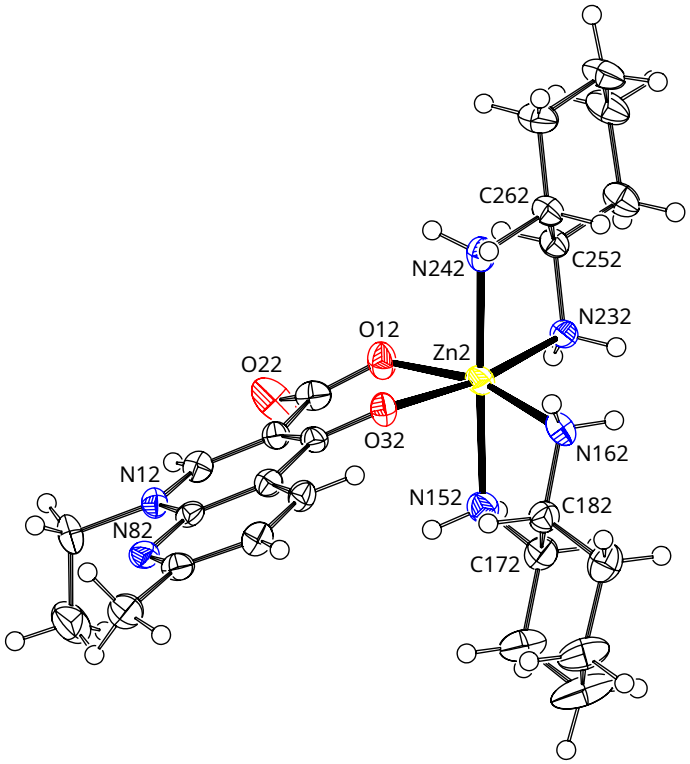

Figure 2. Displacement ellipsoid plot of the monocationic complex molecule at *Zn*2 in **1a** (ellipsoids at the 50% probability level). Atoms C172, C182, C252 and C262 are in *R* configuration. The metal environment has a Δ configuration. The complex at Zn4 is not shown but has the same configuration at the metal and the *DACH* ligands as at Zn2.

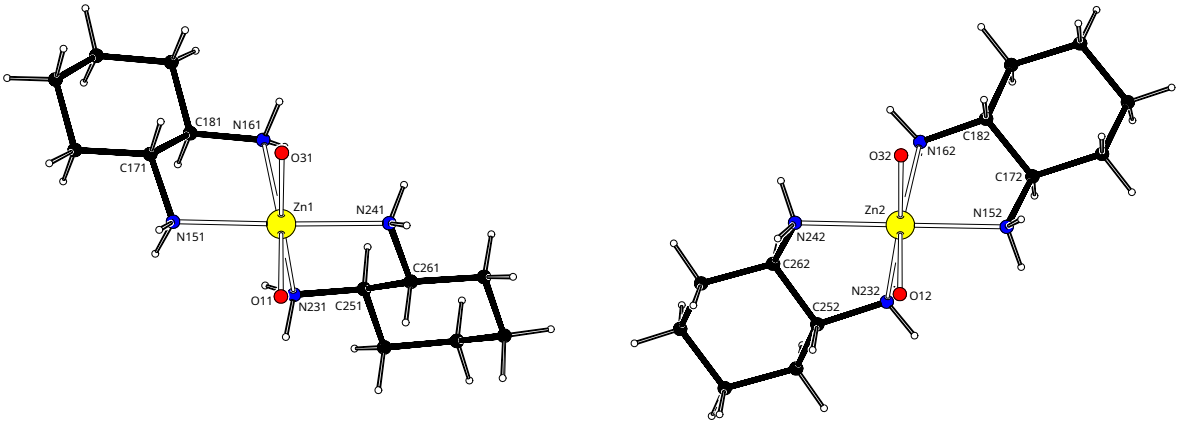

Figure 3. If the *Nal* ligand is ignored, the complexes at Zn1 and Zn2 show approximate C_2 symmetry in **1a**.

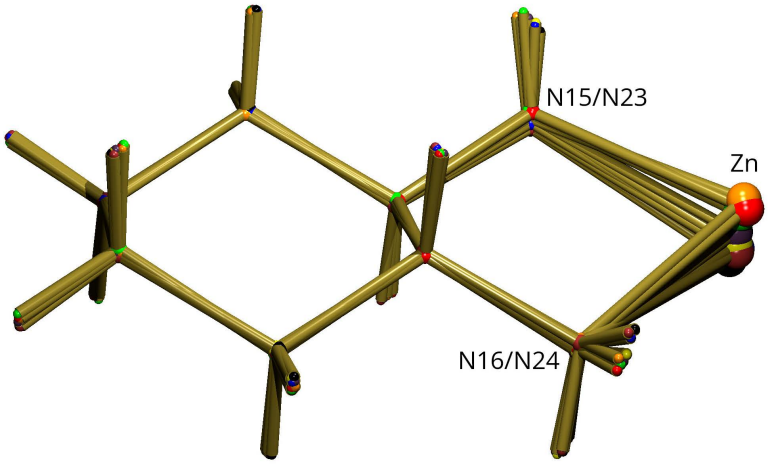

Figure 4. Overlay of the eight independent DACH ligands in **1a**. The calculation of the best fit is based on the cyclohexane rings only.

Table 4. Selected bond distances [Å], angles and torsion angles [°] for the four independent molecules in **1a**.

	x = 1	**x = 2**	**x = 3**	**x = 4**
Zn(x)–O1x	2.115(4)	2.103(4)	2.130(4)	2.126(4)
Zn(x)–O3x	2.123(4)	2.155(4)	2.127(4)	2.133(4)
Zn(x)–N15x	2.162(5)	2.168(5)	2.162(5)	2.172(5)
Zn(x)–N16x	2.173(4)	2.146(5)	2.163(5)	2.149(4)
Zn(x)–N23x	2.137(5)	2.140(5)	2.134(5)	2.129(5)
Zn(x)–N24x	2.158(4)	2.151(5)	2.157(5)	2.166(5)
O1x–Zn(x)–O3x	85.12(15)	83.35(14)	84.59(15)	83.39(15)
N15x–Zn(x)–N16x	81.23(18)	80.47(19)	80.29(18)	80.79(18)
N23x–Zn(x)–N24x	81.73(18)	81.68(18)	81.50(18)	80.92(19)
N15x–C17x–C18x–N16x	−51.8(5)	−53.7(5)	−53.5(5)	−56.6(5)
N23x–C25x–C26x–N24x	−56.6(5)	−54.7(5)	−56.8(5)	−50.5(5)

Table 5. Selected bond distances [Å], angles and torsion angles [°] for the four independent molecules in **1b**.

	x = 1	x = 2	x = 3	x = 4
Zn(x)–O1x	2.120(4)	2.087(4)	2.104(4)	2.096(4)
Zn(x)–O3x	2.135(3)	2.147(3)	2.139(4)	2.139(4)
Zn(x)–N15x	2.166(4)	2.173(4)	2.150(4)	2.159(5)
Zn(x)–N16x	2.166(4)	2.160(4)	2.187(4)	2.145(5)
Zn(x)–N23x	2.125(4)	2.133(4)	2.123(4)	2.129(4)
Zn(x)–N24x	2.147(4)	2.144(4)	2.153(5)	2.139(5)
O1x–Zn(x)–O3x	84.64(13)	84.39(13)	85.44(14)	83.76(14)
N15x–Zn(x)–N16x	80.13(17)	79.54(17)	80.32(17)	80.15(18)
N23x–Zn(x)–N24x	81.57(16)	81.69(16)	81.61(17)	81.34(17)
N15x–C17x–C18x–N16x	−54.3(5)	−53.5(5)	−52.7(5)	−56.6(5)
N23x–C25x–C26x–N24x	−55.1(5)	−55.2(5)	−53.8(5)	−54.5(5)

Obviously, for the full description of the stereochemistry of **1a** and **1b**, the additional chiral elements in the *DACH* ligands need to be considered. The information that all stereocenters of the enantiopure starting material *DACH* are in (R,R) configuration was already known before the synthesis. This is the strongest proof that the structure description of **AYAT** in the centrosymmetric space group $P\bar{1}$ is wrong.

3.2. Crystal Packing

The crystal packing of **1a** and **1b** is characterized by large one-dimensional solvent channels in the direction of the *a*-axis and located at $(x,0,0)$ and $(x,\frac{1}{2},\frac{1}{2})$ (Figure 5). In **1a**, the channels are filled with disordered water molecules, and in **1b** with disordered methanol/water molecules. The volume of the channels in **1b** is slightly larger, leading to a slightly larger unit cell volume overall. After the refinement of the disorder models, there still is residual electron density present. We consider the disorder models reasonable because intermolecular contacts are of acceptable distance and all solvent molecules fit into the hydrogen bonding networks. The residual densities, however, indicate that the disorder model is still approximate.

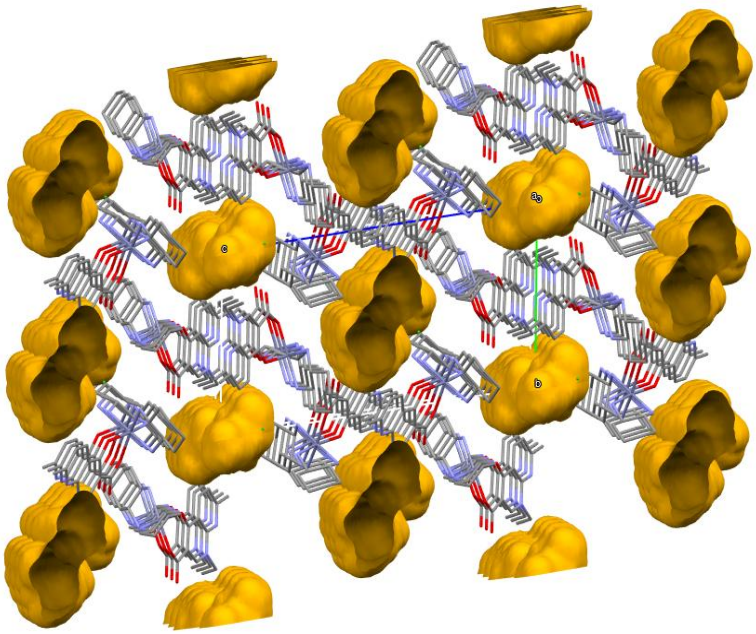

Figure 5. Packing of the molecules in **1a**. Solvent channels are drawn in yellow. View approximately along the *a*-axis. Plot prepared with the Mercury program [21].

In **1a**, the metal complex molecules are linked by hydrogen bonds into one-dimensional chains in the direction of the *b*-axis. Under involvement of the chloride anions and the water molecules, this motif is extended into two-dimensional hydrogen-bonded layers parallel to $hkl = (1, 0, 1)$. Similarly, in **1b**, the metal complex molecules form a hydrogen-bonded chain along the *b*-axis. The chloride anions and methanol/water solvent molecules support this arrangement. Overall, the hydrogen bonding situation in **1b** is one-dimensional. In both **1a** and **1b**, not all NH_2 donor groups have a hydrogen bond acceptor.

In **AYAT**, an analysis of the hydrogen bonding is not possible because the hydrogen atoms are missing in the NH_2 donor groups, and some components of the structure are chemically not identifiable.

The $N - H \cdots Cl$ hydrogen bonds in **1a** and **1b** are rather long (Tables 6 and 7). From a search for hydrogen bonds between metal-coordinated NH_2 groups and free chloride anions in the Cambridge Structural Database [22], one expects a $H \cdots Cl$ distance of $\approx$ 2.47 Å and a $N \cdots Cl$ distance of $\approx$3.31 Å. A typical example is given in [23]. From the long hydrogen bond distances in **1a** and **1b**, we conclude that the chloride anions are only weakly bonded and should be considered a part of the flexible solvent channels. They may even be slightly affected by the disorder in the channels.

Table 6. Geometries of the $N - H \cdots Cl$ hydrogen bonds in **1a**.

$N - H \cdots Cl$	$N - H$ [Å]	$H \cdots Cl$ [Å]	$N \cdots Cl$ [Å]	$N - H \cdots Cl$ [°]
$N161 - H16A \cdots Cl1$	0.91	2.57	3.440(5)	161
$N162 - H16D \cdots Cl2$	0.91	2.60	3.479(5)	163
$N232 - H23D \cdots Cl3$	0.91	2.81	3.548(5)	139
$N163 - H16E \cdots Cl4$	0.91	2.61	3.485(5)	161
$N233 - H23E \cdots Cl1^{\,i}$	0.91	2.76	3.476(5)	136
$N164 - H16H \cdots Cl3$	0.91	2.57	3.456(5)	166
$N234 - H23H \cdots Cl2^{\,ii}$	0.91	2.68	3.468(5)	146

i: $x, y - 1, z$; *ii*: $x, y + 1, z$.

Table 7. Geometries of the $N - H \cdots Cl$ hydrogen bonds in **1b**.

$N - H \cdots Cl$	$N - H$ [Å]	$H \cdots Cl$ [Å]	$N \cdots Cl$ [Å]	$N - H \cdots Cl$ [°]
$N151 - H15A \cdots Cl4$	0.91	2.50	3.341(5)	153
$N241 - H24A \cdots Cl1$	0.91	2.41	3.317(5)	178
$N152 - H15D \cdots Cl3$	0.91	2.51	3.398(5)	166
$N162 - H16D \cdots Cl2$	0.91	2.59	3.422(5)	152
$N232 - H23D \cdots Cl3$	0.91	2.69	3.405(5)	136
$N242 - H24D \cdots Cl2$	0.91	2.35	3.217(5)	158
$N153 - H15E \cdots Cl1^{\,i}$	0.91	2.49	3.348(5)	157
$N243 - H24E \cdots Cl4$	0.91	2.46	3.366(5)	174
$N154 - H15H \cdots Cl2^{\,ii}$	0.91	2.46	3.348(5)	164
$N164 - H16H \cdots Cl3$	0.91	2.73	3.503(5)	144
$N234 - H23H \cdots Cl2^{\,ii}$	0.91	2.54	3.336(5)	146
$N244 - H24H \cdots Cl3$	0.91	2.41	3.272(5)	159

i: $x, y - 1, z$; *ii*: $x, y + 1, z$.

By intermolecular $\pi - \pi$ interactions between the *Nal* ligands, the metal complex molecules form stacked dimers. The complex at Zn1 dimerizes with the one at Zn2, and the complex at Zn3 with that at Zn4. There are *pseudo*-inversion centers between the *Nal* ligand pairs, which makes the stacking arrangement approximately parallel. The *pseudo*-inversion center between the pair Zn1/Zn2 is at $(0, \frac{1}{2}, 0)$ and between the pair Zn3/Zn4, at $(\frac{1}{2}, 0, \frac{1}{2})$. The perpendicular distances between the pairs of *Nal* ligands are approximately 3.3 Å in **1a** and **1b**, respectively.

3.3. Pseudo-Symmetry

Application of the ADDSYM routine of the PLATON software [8] indicates the presence of *pseudo*-inversion symmetry between the molecules. If the disordered solvent is ignored, the fit for the centrosymmetric space group $P\bar{1}$ is 90% for **1a** and 92% for **1b**. The *pseudo*-inversion operation will transform the complex at Zn2 to Zn1 and the complex at Zn4 to Zn3. In other words, it will transform the Λ configuration at the metal on the Δ configuration. After the application of the inversion symmetry to the crystal structure, the six coordinated atoms of the metal octahedron as well as the complete *Nal* ligand fit well. The *DACH* ligands, however, which are ordered in the *P*1 structure, show severe disorder in the $P\bar{1}$ structure (Figure 6). One disorder component of *DACH* has a (R, R) configuration and the other disorder component, a (S, S) configuration. Because of the disorder, the torsion angles of the five-membered chelate rings are not very reliable, but it can be stated that the N–C–C–N torsion angles are in *gauche* conformation and have an approximate magnitude of 60°. In one disorder component of *DACH*, the N–C–C–N torsion has a negative sign and in the other component, a positive sign. As stated above, the (S, S) configuration is not possible with the given synthetic route.

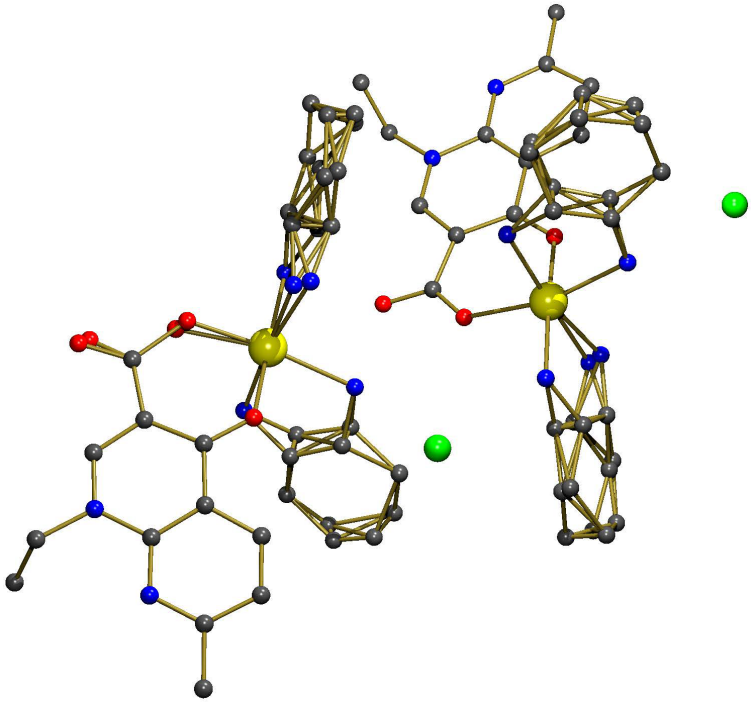

Figure 6. Application of the PLATON-ADDSYM routine to **1a**. Hydrogen atoms and disordered solvent molecules are ignored. Zinc atoms are drawn in yellow, chlorine in green, nitrogen in blue, oxygen in red, and carbon in black. The corresponding figure for **1b** is given in Figure S5 in the Supplementary Materials.

Changing the correct space group *P*1 to the incorrect $P\bar{1}$ in the least-squares refinement worsens the R1 value from 4.0% to approximately 7.9% in **1a**, and from 3.8% to approximately 10.2% in **1b**. More importantly, the refinements in the centrosymmetric space group lead to problems with the scale factor $k = \text{mean}(F^2_{obs})/\text{mean}(F^2_{calc})$ for the weak reflections (Figure 7). It has been shown in the literature that such scale factor deviations for weak reflections are a strong indication for a wrong space group choice in *pseudo*-symmetric cases [11,24,25]. In addition to the chemical knowledge about the synthesis, this is a crystallographic confirmation for the correctness of space group *P*1.

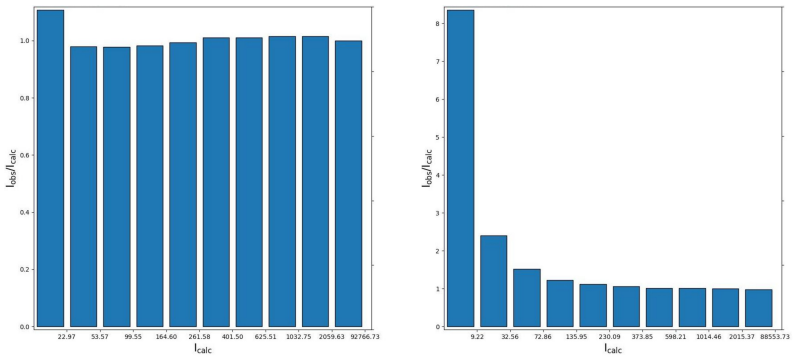

Figure 7. Histogram of the scale factor $k = \text{mean}(F^2_{obs})/\text{mean}(F^2_{calc})$ versus F^2_{calc} in **1a**. The expectation value is $k = 1$ for all reflection groups (reflection bins). The left image is from space group $P1$, the right image from $P\bar{1}$. Plots were prepared with the anafcf software [26]. The corresponding figure for **1b** is given in Figure S6 in the Supplementary Materials.

The presence of *pseudo*-symmetry can lead to an unstable least-squares refinement. This is not the case in **1a** and **1b**. The largest elements in the correlation matrix are only −63.7% for **1a** and −65.1% for **1b** and thus far away from the singularity at 100% or −100%. The metal complex molecules could therefore be refined freely without restraints or constraints. The resulting standard uncertainties in the bond geometries are fairly low (Tables 4 and 5). Normal probability plots for the bond distances in the metal complexes are reasonable (Figures S7 and S8 in the Supplementary Materials) with slopes between 1.18 and 1.92 for **1a** and between 1.36 and 2.18 for **1b**. Outliers in the plots are moderate. It is thus possible to analyze the bond distances reliably (Tables 4 and 5). The shortest Zn–N distance is consistently Zn–N23 with an average of 2.135(2) Å for **1a** and 2.128(2) Å for **1b**. Thereby, N23 is located *trans* to the keto-oxygen O3 of the *Nal* ligand. The other Zn–N distances vary significantly between 2.146(5) and 2.173(4) Å for **1a** and between 2.144(4) and 2.187(4) Å for **1b**. As expected, the angles at the metal deviate from the perfect octahedron due to the bite angles of the chelating ligands.

As a consequence of the *pseudo*-inversion symmetry, the absolute structure determination becomes a challenge. The phase angles of the structure factors accumulate at values of 0 and 180°, which is very similar to the centrosymmetric case, where the values of 0 and 180° are obviously exact (see Figure S9 in the Supplementary Materials).

The 2AD-plot was introduced by [27], with A being the average of $F^2(h,k,l)$ and $F^2(\bar{h},\bar{k},\bar{l})$ and D being the difference between $F^2(h,k,l)$ and $F^2(\bar{h},\bar{k},\bar{l})$. Here, this plot shows an accumulation of Friedel pairs at $D_{model} \approx 0$ and a large variation of D_{obs} (Figure 8). We conclude that a large number of reflections contain little or no information about the absolute structure. In fact, in **1a**, only 40.1% of all Friedel pairs have $|D_{obs}| > 1\sigma$ and only 6.4% have $|D_{obs}| > 3\sigma$. For **1b**, the corresponding percentages are 36.5% and 4.9%. The information content is thus much smaller than, for example, in the archetypical Na-Rb-(+)-tartrate when measured with modern equipment [28], where we find 70.5% for $> 1\sigma$ and still 36.3% for $> 3\sigma$. The difficulty in the absolute structure determination of **1a** and **1b** using the Parsons z-parameter [16] and the Hooft y-parameter [17] can be seen in Table 1, where the found values can deviate significantly from the expected value of *zero*, and the standard uncertainties of z and y are apparently underestimated. The most reliable result for the absolute structure determination, here, is obtained from the Flack x-parameter, which is obtained from a refinement as an inversion twin [15].The x-parameter in **1a** and **1b** confirms the enantiopurity and thus the absence of centrosymmetry.

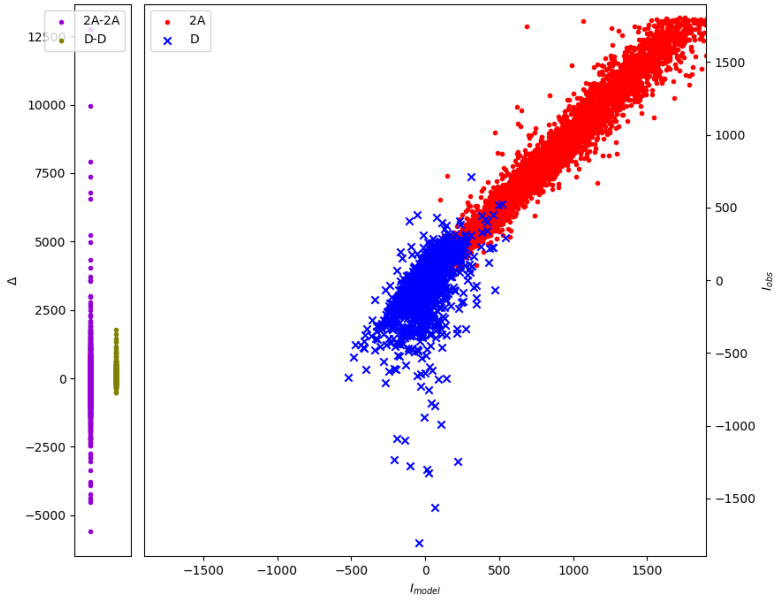

Figure 8. A 2AD plot for **1a** according to [27]. In the right panel, the difference values D are plotted in blue for all Friedel pairs. The average values $2A$ are plotted in red for the weak reflections only. The values for I_{model} are taken from the non-twinned F^2_{calc} of the single crystal. The left panel shows $D_{obs} - D_{model}$ and $2A_{obs} - 2A_{model}$ for all Friedel pairs. The corresponding figure for **1b** is given in Figure S10 in the Supplementary Materials.

The treatment of the diffuse electron density of disordered solvent molecules with the Squeeze algorithm [18] improves the structural results for **1a** and **1b**. Both the refined R-values and the residual electron density improve (Table 2). In the input files for Squeeze, the water and methanol molecules are considered disordered and were removed from the coordinate list. In principle, the chlorine atoms are also in the solvent channel and they might be part of the disorder. Nevertheless, they were assigned to the ordered part of the structure. The chlorine atoms are significant anomalous scatterers and a removal could bias the Squeeze calculation which is based only on the real part of the structure factors F. The imaginary part (i.e, the resonant scattering) is ignored [29]. In the case of **1a** and **1b**, the Squeeze procedure for water and methanol does not improve the absolute structure determination. Table S3 in the Supplementary Materials shows the R-value changes from the application of Squeeze. Squeeze improves R_A, which is a classical R-value based on the Friedel averages A. R_D, which is based on the Friedel differences D, is not changed by Squeeze.

We can only speculate as to why the authors in [4] have chosen the wrong space group $P\bar{1}$ despite the enantiopure synthesis. The most probable reason is the use of automatic software packages for X-ray crystal structure determination. They are available as components of automated diffractometers or as stand-alone programs, and their purpose is to simplify routine tasks, also for the non-specialist. Traditionally, the first step of the structure analysis is the determination of the space group. This is based on systematic absences. In the case of ambiguities and in the triclinic crystal system without systematic absences, statistical methods for the intensity distributions can be applied. Both the $|E^2 - 1|$ and the $N(Z)$ statistics strongly indicate a centrosymmetric space group (Figures S11 and S12 in the Supplementary Materials). Consequently, space group routines in PLATON [8] or in the XPREP software [30] will give the highest probability to space group $P\bar{1}$. (Both programs only give a proposal for the space group, and the user needs to decide. The XPREP software has the possibility to restrict the search to Sohncke space groups.) A more modern approach is to solve the phase problem with dual-space methods in space group $P1$ without symmetry information. The space group is then determined from the results. The module Flip in PLATON [8] is an implementation of the charge flipping algorithm [31]. PLATON

assigns atoms to the structure solution and then uses ADDSYM to find the space group. The automatic result is $P\bar{1}$. Another implementation of the charge flipping method is in the SUPERFLIP software [32]. Here, the symmetry is derived from the electron density and gives *symmetry agreement factors* for **1a** and **1b**, indicating a very good agreement with $P\bar{1}$. (The manual of SUPERFLIP has an explicit warning that it is impossible to determine the correct agreement factor for all situations automatically.) The intrinsic phasing approach in SHELXT [33] solves the phase problem by dual-space iterations. The space group is then determined from the phase relationships of the structure factors. Table S4 in the Supplementary Materials gives the output of SHELXT with acceptable agreement factors for both space groups $P1$ and $P\bar{1}$. It is then the decision of the user if the quality difference is significant enough to choose the lower symmetry.

4. Conclusions

In this study, the compound $[Zn(NaI)(DACH)_2]Cl$ has been re-synthesized and the identity with structure **AYAT** from [4] has been proven. The wrong space group of $P\bar{1}$ for **AYAT** has been changed to the correct space group $P1$ for **1a** and **1b**. The latter is a Sohncke space group and thus compatible with the enantiopure starting material. With this correction, the originally severely disordered structure in **AYAT** becomes well ordered in **1a** and **1b**. This allows a detailed analysis of intra- and intermolecular geometries of the metal complex. The crystal structures **1a** and **1b** contain one-dimensional solvent channels for which an appropriate disorder model was found. The current report is a warning to remain critical when automatic crystallographic software is used. Software authors invest a lot of effort, but the final responsibility is with the program users. The training of chemists in this respect is essential [34]. This report is also a reminder to reviewers and journal editors that the space group choice is not a minor side issue but essential for the correct structure description.

Supplementary Materials: The following supporting information can be downloaded at: https://www.mdpi.com/article/10.3390/cryst14060498/s1. Figure S1: Crystals of **1a** (left) and **1b** (right) mounted with perfluoroalkyl ether oil on MiTeGen loops for X-ray data collection; Figure S2: Approximate shape of **1a**. Figure from PLATON [8]; Figure S3: Approximate shape of **1b**. Figure from PLATON [8]; Figure S4: Arrangement of zinc atoms (yellow) and chlorine atoms (green) in the unit cells of **AYAT** (top), **1a** (middle) and **1b** (bottom). View along the b-axis, respectively. Plot prepared with PLATON [8]; Figure S5: Application of the PLATON-ADDSYM routine [8] to **1b**. Hydrogen atoms and disordered solvent molecules are ignored. Zinc atoms are drawn in yellow, chlorine in green, nitrogen in blue, oxygen in red, and carbon in black; Figure S6: Histogram of the scale factor k = mean(F^2_{obs})/mean(F^2_{calc}) versus F^2_{calc} in **1b**. Expected value is k = 1 for all reflection groups (reflection bins). The left image is from space group $P1$, the right image from $P\bar{1}$. Plots were prepared with the anafcf software [26]. Figure S7: Normal probability plots [35] for the comparison of 40 individual bond distances in the octahedral Zn-complex molecules in **1a**; Figure S8: Normal probability plots [35] for the comparison of 40 individual bond distances in the octahedral Zn-complex molecules in **1b**; Figure S9: Distribution of the phase angles of the calculated structure factors in **1a** (top). For comparison, the phase angles of the centrosymmetric refinement are given (bottom); Figure S10: 2AD plot [27] for **1b**; Figure S11: $|E^2 - 1|$ statistics [36] for **1a** (top) and **1b** (bottom). The black horizontal line at 0.968 is the expectation value for a centrosymmetric structure and at 0.736 for a non-centrosymmetric structure. The experimental values are drawn in blue. The plots were created with the SADABS program [13]. Figure S12: $N(Z)$ statistics [37] for **1a** (top) and **1b** (bottom). The distributions were calculated with the PLATON program [8]; Table S1: Puckering analysis of the five-membered chelate rings in **1a**. According to [38] the puckering can be described as linear combination of the cos form (envelope form) and the *sin* form (twist form). The corresponding coefficients of the normalised forms are given in this table; Table S2: Puckering analysis of the five-membered chelate rings in **1b**. According to [38] the puckering can be described as linear combination of the cos form (envelope form) and the *sin* form (twist form). The corresponding coefficients of the normalised forms are given in this table; Table S3: Friedel pair R-values [27]. R_A is based on the average F^2 of the Friedel pairs. R_D is based on the difference of F^2 of the Friedel pairs; Table S4: Space group determination with SHELXT [33].

Author Contributions: Conceptualization , M.L.; formal analysis, M.L.; data curation, M.L., T.W.M.; writing—original draft preparation, M.L.; writing—review and editing, M.L., T.W.M. All authors have read and agreed to the published version of the manuscript.

Funding: The X-ray diffractometer was financed by the Netherlands Organization for Scientific Research (NWO).

Institutional Review Board Statement: Not applicable.

Informed Consent Statement: Not applicable.

Data Availability Statement: CCDC 2352729 (crystal structure **1a**), 2352730 (**1a-squeeze**), 2352731 (**1b**) and 2352732 (**1b-squeeze**) contain the supplementary crystallographic data for this paper. These data can be obtained free of charge from The Cambridge Crystallographic Data Centre via www.ccdc.cam.ac.uk/data_request/cif, accessed on 1 May 2024.

Conflicts of Interest: The authors declare no conflicts of interest.

Abbreviations

The following abbreviations are used in this manuscript:

DACH	Diaminocyclohexane
NalH	Nalidixic acid
Nal	Deprotonated nalidixic acid (mono-anion)

References

1. Bennani, Y.L.; Hanessian, S. trans-1,2-Diaminocyclohexane Derivatives as Chiral Reagents, Scaffolds, and Ligands for Catalysis: Applications in Asymmetric Synthesis and Molecular Recognition. *Chem. Rev.* **1997**, *97*, 3161–3196. https://doi.org/10.1021/cr9407577.
2. Zhu, G.; Jiang, D.; Yang, Q.; Yang, J.; Li, C. trans-(1R,2R)-Diaminocyclohexane-functionalized mesoporous organosilica spheres as chiral stationary phase. *J. Chromatogr.* **2007**, *1149*, 219–227. https://doi.org/10.1016/j.chroma.2007.03.011.
3. Zheng, C.; er Chen, F. An efficient method for the resolution of rac-VANOL by molecular complexation with (1S,2S)-(+)-diaminocyclohexane. *Tetrahedron Asymmetry* **2014**, *25*, 792–795. https://doi.org/10.1016/j.tetasy.2014.04.016.
4. Arjmand, F.; Yousuf, I.; Afzal, M.; Toupet, L. Design and synthesis of new Zn(II) nalidixic acid-DACH based Topo-II inhibiting molecular entity: Chemotherapeutic potential validated by its in vitro binding profile, pBR322 cleavage activity and molecular docking studies with DNA and RNA molecular targets. *Inorganica Chim. Acta* **2014**, *421*, 26–37. https://doi.org/10.1016/j.ica.2014.05.015.
5. Nye, J.F. *Physical Properties of Crystals Their Representation by Tensors and Matrices*; Oxford Science Publications, Clarendon Press: Oxford, UK, 2012.
6. Cen, Z.; Li, F.; Wei, J.; Gao, Z.; Liu, Z.; Zhang, T.; Han, D.; Chen, M.; Gong, J. Recent Advances in the Asymmetric Growth of Organic Polar Crystals: A Review. *Cryst. Growth Des.* **2023**, *23*, 7517–7534. https://doi.org/10.1021/acs.cgd.3c00425.
7. Clemente, D.A. A study of the 8466 structures reported in Inorganica Chimica Acta: 52 space group changes and their chemical consequences. *Inorganica Chim. Acta* **2005**, *358*, 1725–1748. https://doi.org/10.1016/j.ica.2004.10.037.
8. Spek, A.L. Structure validation in chemical crystallography. *Acta Crystallogr. Sect. D* **2009**, *65*, 148–155. https://doi.org/10.1107/S090744490804362X.
9. Harlow, R.L. Troublesome Crystal Structures: Prevention, Detection, and Resolution. *J. Res. Natl. Inst. Stand. Technol.* **1996**, *101*, 327–339. https://doi.org/10.6028/jres.101.034.
10. Nespolo, M.; Benahsene, A.H. Symmetry and chirality in crystals. *J. Appl. Crystallogr.* **2021**, *54*, 1594–1599. https://doi.org/10.1107/S1600576721009109.
11. Lutz, M. Comment on "Crystallographic and theoretical study of the atypical distorted octahedral geometry of the metal chromophore of zinc(II) bis((1R,2R)-1,2-diaminocyclohexane) dinitrate". *J. Mol. Struct.* **2023**, *1284*, 135362. https://doi.org/10.1016/j.molstruc.2023.135362.
12. Schreurs, A.M.M.; Xian, X.; Kroon-Batenburg, L.M.J. *EVAL15*: A diffraction data integration method based on *ab initio* predicted profiles. *J. Appl. Crystallogr.* **2010**, *43*, 70–82. https://doi.org/10.1107/S0021889809043234.
13. Krause, L.; Herbst-Irmer, R.; Sheldrick, G.M.; Stalke, D. Comparison of silver and molybdenum microfocus X-ray sources for single-crystal structure determination. *J. Appl. Crystallogr.* **2015**, *48*, 3–10. https://doi.org/10.1107/S1600576714022985.
14. Sheldrick, G.M. Crystal structure refinement with *SHELXL*. *Acta Crystallogr. Sect. C* **2015**, *71*, 3–8. https://doi.org/10.1107/S2053229614024218.
15. Flack, H.D. On enantiomorph-polarity estimation. *Acta Crystallogr. Sect. A* **1983**, *39*, 876–881. https://doi.org/10.1107/S0108767383001762.

16. Parsons, S.; Flack, H.D.; Wagner, T. Use of intensity quotients and differences in absolute structure refinement. *Acta Crystallogr. Sect. B* **2013**, *69*, 249–259. https://doi.org/10.1107/S2052519213010014.
17. Hooft, R.W.W.; Straver, L.H.; Spek, A.L. Determination of absolute structure using Bayesian statistics on Bijvoet differences. *J. Appl. Crystallogr.* **2008**, *41*, 96–103. https://doi.org/10.1107/S0021889807059870.
18. Spek, A.L. *PLATON* SQUEEZE: a tool for the calculation of the disordered solvent contribution to the calculated structure factors. *Acta Crystallogr. Sect. C* **2015**, *71*, 9–18. https://doi.org/10.1107/S2053229614024929.
19. de la Flor, G.; Orobengoa, D.; Tasci, E.; Perez-Mato, J.M.; Aroyo, M.I. Comparison of structures applying the tools available at the Bilbao Crystallographic Server. *J. Appl. Crystallogr.* **2016**, *49*, 653–664. https://doi.org/10.1107/S1600576716002569.
20. Ehnbom, A.; Ghosh, S.K.; Lewis, K.G.; Gladysz, J.A. Octahedral Werner complexes with substituted ethylenediamine ligands: a stereochemical primer for a historic series of compounds now emerging as a modern family of catalysts. *Chem. Soc. Rev.* **2016**, *45*, 6799–6811. https://doi.org/10.1039/C6CS00604C.
21. Macrae, C.F.; Edgington, P.R.; McCabe, P.; Pidcock, E.; Shields, G.P.; Taylor, R.; Towler, M.; van de Streek, J. *Mercury*: visualization and analysis of crystal structures. *J. Appl. Crystallogr.* **2006**, *39*, 453–457. https://doi.org/10.1107/S002188980600731X.
22. Groom, C.R.; Bruno, I.J.; Lightfoot, M.P.; Ward, S.C. The Cambridge Structural Database. *Acta Crystallogr. Sect. B* **2016**, *72*, 171–179. https://doi.org/10.1107/S2052520616003954.
23. Moon, D.; Choi, J.H. Crystal structure of tris(*trans*-1,2-cyclohexanediamine-κ^2N,N')chromium(III) tetrachloridozincate chloride trihydrate from synchrotron data. *Acta Crystallogr. Sect. E* **2016**, *72*, 671–674. https://doi.org/10.1107/S2056989016005788.
24. Walker, M.; Pohl, E.; Herbst-Irmer, R.; Gerlitz, M.; Rohr, J.; Sheldrick, G.M. Absolute configurations of Emycin D, E and F; mimicry of centrosymmetric space groups by mixtures of chiral stereoisomers. *Acta Crystallogr. Sect. B* **1999**, *55*, 607–616. https://doi.org/10.1107/S0108768199003948.
25. Huang, Y.; Moret, M.E.; Klein Gebbink, R.J.M.; Lutz, M. Crystallographic Space Group Choice and Its Chemical Consequences: Revised Crystal Structure of $[Fe(phen)_2Cl)_2]NO)_3$. *Eur. J. Inorg. Chem.* **2013**, *2013*, 2467–2469. https://doi.org/https://doi.org/10.1002/ejic.201201452.
26. Schreurs, A.M.M.; Lutz., M. *anafcf*; Utrecht University: Utrecht, The Netherlands, 2022. http://www.crystal.chem.uu.nl/distr
27. Parsons, S.; Pattison, P.; Flack, H.D. Analysing Friedel averages and differences. *Acta Crystallogr. Sect. A* **2012**, *68*, 736–749. https://doi.org/10.1107/S0108767312034885.
28. Lutz, M.; Schreurs, A.M.M. Was Bijvoet right? Sodium rubidium (+)-tartrate tetrahydrate revisited. *Acta Crystallogr. Sect. C* **2008**, *64*, m296–m299. https://doi.org/10.1107/S0108270108022415.
29. Cooper, R.I.; Flack, H.D.; Watkin, D.J. HUG and SQUEEZE: using *CRYSTALS* to incorporate resonant scattering in the SQUEEZE structure-factor contributions to determine absolute structure. *Acta Crystallogr. Sect. C* **2017**, *73*, 845–853. https://doi.org/10.1107/S2053229617013304.
30. Bruker AXS Inc. *XPREP*.; Bruker AXS Inc.: Madison, WI, USA, 2012.
31. Oszlányi, G.; Süto, A. *Ab initio* structure solution by charge flipping. *Acta Crystallogr. Sect. A* **2004**, *60*, 134–141. https://doi.org/10.1107/S0108767303027569.
32. Palatinus, L.; Chapuis, G. *SUPERFLIP*—A computer program for the solution of crystal structures by charge flipping in arbitrary dimensions. *J. Appl. Crystallogr.* **2007**, *40*, 786–790. https://doi.org/10.1107/S0021889807029238.
33. Sheldrick, G.M. *SHELXT*—Integrated space-group and crystal-structure determination. *Acta Crystallogr. Sect. A* **2015**, *71*, 3–8. https://doi.org/10.1107/S2053273314026370.
34. Campbell, M.G.; Powers, T.M.; Zheng, S.L. Teaching with the Case Study Method To Promote Active Learning in a Small Molecule Crystallography Course for Chemistry Students. *J. Chem. Educ.* **2016**, *93*, 270–274. https://doi.org/10.1021/acs.jchemed.5b00629.
35. Abrahams, S.C.; Keve, E.T. Normal probability plot analysis of error in measured and derived quantities and standard deviations. *Acta Crystallogr. Sect. A* **1971**, *27*, 157–165.
36. Rupp, B. *Biomolecular Crystallography*; Garland Science: New York, NY, USA, 2010; pp. 354–355.
37. Howells, E.R.; Phillips, D.C.; Rogers, D. The probability distributionof X-ray intensities. II. Experimental investigation and the X-ray detection of centres of symmetry. *Acta Crystallogr.* **1950**, *3*, 210–214.
38. Evans, D.G.; Boeyens, J.C.A. Conformational analysis of ring pucker. *Acta Crystallogr. Sect. B* **1989**, *45*, 581–590.